HEAT 2008, Fifth International Conference on
Transport Phenomena In Multiphase Systems
June 30 - July 3, 2008, Bialystok, Poland

A Numerical Study on Bubble Rise and Interaction in a Viscous Liquid

Mohammad Passandideh-Fard[1] and Mehran M. Farhangi[2]

[1]Assistant Professor, Ferdowsi University of Mashhad, Iran, (mpfard@um.ac.ir),
[2]Graduate Student, Ferdowsi University of Mashhad, Iran, (farhangi.mehran@gmail.com)

Abstract

In this paper, the rising of a single bubble and coalescence of two co-axial gas bubbles in a viscous liquid are simulated using a transient 2D/axisymmetric model. To predict the shape of the bubble deformation, Navier-Stokes equations in addition to an advection equation for liquid volume fraction are solved. A modified Volume-of-Fluid (VOF) technique based on Youngs' algorithm is used to track the bubble deformation. To validate the model, the results of simulations for terminal rise velocity and bubble shape are compared with those of the experiments. Next, the effect of different parameters such as initial bubble radius, channel height, and liquid viscosity and surface tension on the shape and rise velocity of the bubble is investigated**.** Finally, the interaction of two co-axial gas bubbles in a liquid is simulated, and the computed bubble shapes are compared with experimental observations.

Keywords: *bubble rise, bubble interaction, bubble coalescence, bubble shape, Numerical Simulation***,** *Volume-of-Fluid*

INTRODUCTION

The motion and interaction of drops and bubbles in a continuous phase are frequently encountered in many industrial applications such as food processing, production of lubricant oils, paints, and pharmaceutical and cosmetic products. In several operations such as polymerization processes, dispersion, extraction, enhanced oil recovery, and production of detergents, bubble motion is often accompanied by heat and mass transfer and/or a chemical reaction. An associated phenomenon that plays a significant role in all these operations is bubble coalescence. There are instances where it is desirable for coalescence to occur, as in the case of separation process, while in other cases coalescence is a highly undesirable process. For example, during a gas-liquid reaction, the coalescence of gas bubbles results in a reduction in interfacial area and thus reduces the efficiency of the reactor.

In the past decade, a number of techniques, each with its own particular advantages and disadvantages, have been developed to simulate complex multi-fluid flow problems.

Level set methods (Sussman et al., 1994; Sethian, 1996; Chang et al., 1996; Sussman and Smereka, 1997; Sussman and Fatemi, 1999; Fedkiw and Osher, 2001) are designed to minimize the numerical diffusion hampering shock-capturing methods and typically define the interface as the zero level set of a distance function from the interface. The advection of this distance function evolves with the local fluid velocity. Level set methods are conceptually simple and relatively easy to implement. When the interface is significantly deformed, level set methods suffer from loss of mass (volume) and hence loss of accuracy.

A well-known method for tracking the free surface of a liquid is Volume-of-Fluid (VOF) technique (Passandideh-Fard and Roohi, 2008) where the computational domain is characterized by a liquid volume fraction function. This function is used to determine both the liquid position and the liquid/gas interface orientation. Roughly two important classes of VOF methods can be distinguished with respect to the representation of the interface, namely simple line interface calculation (SLIC) and piecewise linear interface calculation (PLIC). Earlier works with VOF were generally based on the SLIC algorithm introduced by Noh and Woodward (1976) and the donor-acceptor algorithm published by Hirt and Nicholas (1981). More accurate VOF techniques include the PLIC method of Youngs (1982). The accuracy and capabilities of the older VOF algorithm such as the Hirt-and-Nicholas VOF method were studied by Rudman, 1997.

Front tracking methods (Unverdi and Tryggvason, 1992; Esmaeeli and Tryggvason, 1998a, 1998b; Tryggvasson et al., 2001) make use of markers (for instance triangles), connected to a set of points, to track the interface whereas a fixed or Eulerian grid is used to solve the Navier-stokes equations. This method is extremely accurate but also rather complex to implement due to the fact that dynamic re-meshing of the Lagrangian interface mesh is required and mapping of the Lagrangian data onto the Eulerian mesh has to be carried out. Difficulties arise when multiple interfaces interact where all require a proper sub-grid model. Contrary to most other methods, the automatic merging of interfaces does not occur in front tracking techniques due to the fact that a separate mesh is used to track the interface. 3D front tracking method was used by Van Sint Annaland et al. (2006) to simulate a single bubble rising in water. The front tracking algorithm predicted reasonably well the rise velocity and aspect ratio of a single air bubble rising in water for diameters in the range of 1to 7 mm.

Experimental studies of the interaction and coalescence of two fluid particles in pure liquids are very limited. Only a few

experimental studies have been reported in the literature dealing with buoyancy-driven interaction and coalescence of two fluid particles under low Reynolds number conditions. Olbricht and Kung (1987) experimentally studied the interaction between two liquid drops of unequal size suspended in low Reynolds number flow through a capillary tube. Most recently, Manga and Stone (1993) studied the non-axisymmetric buoyancy driven interaction of two air bubbles rising in a large container filled with corn syrup. They observed that the initial horizontal displacement of the two deformable bubbles determines the type of bubble interaction that occurs. The in-line interaction of two gas bubbles rising in an unbounded fluid domain was experimentally studied by Crabtree and Bridgewater(1971), Narayanan et al.(1974) and Bhaga and Weber (1980). These studies showed that the wake of the leading bubble can play a vital role both in capturing non-aligned bubbles and in the subsequent coalescence behavior of the bubbles. Duineveld (1998) experimentally investigated the behavior of two bubbles rising side by side in hyper filtrated water.

In this study, the rising of a single bubble and coalescence of two co-axial gas bubbles in a viscous liquid are simulated using a transient 2D/axisymmetric model. A modified Volume-of-Fluid (VOF) technique based on Youngs' algorithm is used to track the bubble deformation. To validate the model, numerical results are compared with those of the experiments for terminal rise velocity and bubble shape. The effect of different parameters such as initial bubble radius, channel height, and liquid viscosity and surface tension on the shape and rise velocity of the bubble is investigated**.**

NUMERICAL METHOD

The main issue regarding the developed model is the advection of the bubble interface using VOF method. In this section, we present a brief account of the numerical method. The flow governing equations are:

$$\vec{\nabla}\cdot\vec{V}=0 \tag{1}$$

$$\frac{\partial\vec{V}}{\partial t}+\vec{\nabla}\cdot(\vec{V}\vec{V})=-\frac{1}{\rho}\vec{\nabla}p+\frac{1}{\rho}\vec{\nabla}\cdot\vec{\tau}+\frac{1}{\rho}\vec{F}_b \tag{2}$$

where $\vec{V}$ is the velocity vector, p is the pressure and $\vec{F}_b$ represents body forces acting on the fluid. The bubble interface is advected using VOF method by means of a scalar field f whose value is unity in the liquid phase and zero in the gas. When a cell is partially filled with liquid, f will have a value between zero and one.

$$f=\begin{cases}1 & \text{in liquid}\\ >0,<1 & \text{at the liquid-gas interface}\\ 0 & \text{in gas}\end{cases} \tag{3}$$

The discontinuity in f is propagating through the computational domain according to:

$$\frac{df}{dt}=\frac{\partial f}{\partial t}+\vec{V}\cdot\vec{\nabla}f=0 \quad\Rightarrow\quad (\frac{\partial f}{\partial t})_{exact}=-(\vec{V}.\vec{\nabla})f \tag{4}$$

Although the velocity field is divergence free, the term $(\vec{\nabla}\cdot\vec{V})$ has an order of $O(\varepsilon)$ in numerical solution. Therefore, in order to increase the accuracy of the numerical solution, Eq. 4 is used in the conservative form as

$$(\frac{\partial f}{\partial t})_{numerical}=-(\vec{V}.\vec{\nabla})f-(\vec{\nabla}\cdot\vec{V})f=-\vec{\nabla}\cdot(\vec{V}f) \tag{5}$$

where

$$(\frac{\partial f}{\partial t})_{exact}=(\frac{\partial f}{\partial t})_{numerical}+(\vec{\nabla}\cdot\vec{V})f \tag{6}$$

For the advection of volume fraction f based on Eq. 4, different methods have been developed such as SLIC, Hirt-Nichols and Youngs' PLIC. The reported literature on the simulation of free-surface flows reveals that the Hirt-Nichols method has been used by many researchers. In this study, however, we used Youngs' method (Passandideh-Fard and Roohi, 2008; Bussmann et al., 1999), which is a more accurate technique. Assuming the initial distribution of f to be given, velocity and pressure are calculated in each time step by the following procedure. The f advection begins by defining an intermediate value of f,

$$\tilde{f}=f^n-\delta t\vec{\nabla}\cdot(\vec{V}f^n) \tag{7}$$

Then it is completed with a "divergence correction"

$$f^{n+1}=\tilde{f}+\delta t(\vec{\nabla}\cdot\vec{V})f^n \tag{8}$$

A single set of equations is solved for both phases, therefore, density and viscosity of the mixture are calculated according to:

$$\begin{aligned}\rho&=f\rho_l+(1-f)\rho_g\\ \mu&=f\mu_l+(1-f)\mu_g\end{aligned}, \tag{9}$$

where subscripts l and g denote the liquid and gas, respectively. New velocity field is calculated according to the two-step time projection method as follows. First, an intermediate velocity is obtained,

$$\frac{\tilde{\vec{V}}-\vec{V}^n}{\delta t}=-\vec{\nabla}\cdot(\vec{V}\vec{V})^n+\frac{1}{\rho^n}\vec{\nabla}\cdot\vec{\tau}^n+\vec{g}^n+\frac{1}{\rho^n}\vec{F}_b{}^n \tag{10}$$

The continuum surface force (CSF) method (Bussmann et al., 1999) is used to model surface tension as a body force ($\vec{F}_b$) that acts only on interfacial cells. A pressure Poisson equation is then solved to obtain the pressure field,

$$\vec{\nabla}\cdot[\frac{1}{\rho^n}\vec{\nabla}p^{n+1}]=\frac{\vec{\nabla}\cdot\tilde{\vec{V}}}{\delta t} \tag{11}$$

Next, new time velocities are calculated by considering the pressure field implicitly,

$$\frac{\vec{V}^{n+1}-\tilde{\vec{V}}}{\delta t}=-\frac{1}{\rho^n}\vec{\nabla}p^{n+1} \tag{12}$$

The cell size used in this study was set based on a mesh refinement study in which the grid size was progressively increased until no significant changes were observed in the simulation results. The mesh resolution was characterized by the number of cells per the bubble diameter. From the mesh refinement study, the optimum mesh size was found to be 15 cells per bubble radius. This mesh sized was used for all simulations throughout this paper.

RESULTS AND DISCUSSION

As a first step, the model was subjected to several tests in order to validate its results. The first case considered was that of a single bubble during its rise in a liquid; a case for which experimental results are available in terms of terminal bubble rise velocity against its diameter. The measured data performed by Grace (1973) for air bubbles in water is given as a diagram shown in Fig. 1. The default material properties used in the simulations are given in Table 1.

Table 1. Material properties.

properties	water	air
density	ρ_l=998.2 kg/m^3	ρ_a=1.1222 kg/m^3
viscosity	μ_l=1002×10^{-6} kg/(m.s)	μ_a=18.24×10^{-6} kg/(m.s)
surface tension	γ =0.073 N/m	

An axisymmetric coordinate system was used in the model to simulate the deformation of the bubbles rising in a vertical tube. The tube diameter was assumed to be around four times as that of the bubble diameter in order to reduce the wall influence on bubble movement. Bubbles with diameter ranged from 0.8 mm to 10 mm were simulated. Larger bubbles broke up before they reached their terminal velocity.

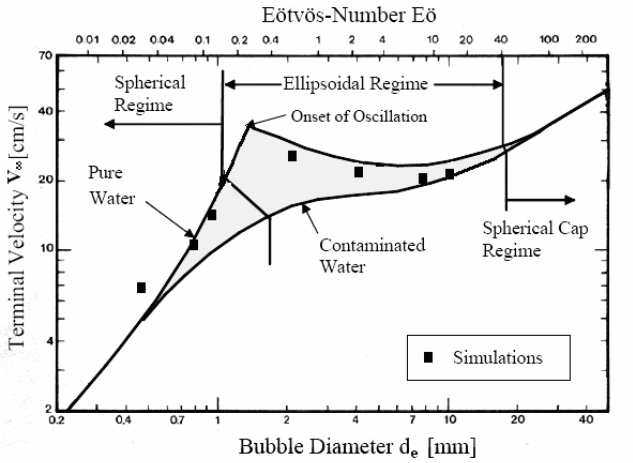

Fig. 1. A comparison between the results of simulations with those of the experiments (Clift et al.; 1978) for terminal rise velocity against initial bubble diameter. Based on the experiments, the rise velocity should be located in the region surrounded by the solid lines.

The results of the model, presented in the same figure (Fig. 1), are located in the same region where observed by experiments. The upper boundary of this region corresponds to pure systems, while the lower curve belongs to contaminated systems. As seen from the figure, increasing the bubble diameter increases the rise velocity up to a certain limit after which the bubble starts to oscillate. In this regime, the rise velocity remains nearly constant. Adding further to the bubble diameter changes the deformation behavior to the spherical cap regime where the rise velocity again increases with diameter. As it can be seen from Fig. 1, for the bubbles smaller than the 0.5 mm there is an increasing deviation of simulated to measured velocities, which occurs mainly because of the so-called parasitic currents. These currents are due to inaccuracies in treating surface tension forces, in particular because of errors in the calculation of the interfacial normal vector and curvature.

Model Validation

Grace has analyzed a large body of experimental data on shapes and rise velocities of bubbles in quiescent viscous liquids and has shown that this data can be condensed into one diagram, provided that an appropriate set of dimensionless numbers is used. A representation of the Grace diagram is shown in Fig. 2 where dimensionless numbers Morton (M), Eötvös (Eo), and Reynolds (Re) are given by

$$\mathrm{M}=\frac{\Delta\rho g\mu_l^4}{\rho_l^2\gamma^3},\qquad \mathrm{Eo}=\frac{\Delta\rho g d_e^2}{\gamma},\qquad \mathrm{Re}=\frac{\rho_l V_\infty d_e}{\mu_l} \tag{13}$$

where the equivalent diameter d_e is defined as the diameter of a spherical bubble with the same volume as that of the bubble under consideration. V_∞ represents the terminal rise velocity of the bubble.

In Table 2, the values of the selected Morton and Eötvös numbers are given for simulations of bubbles in different regimes according to this diagram. In this table, Re_{exp} and Re_{model} represent the bubble Reynolds numbers obtained from Grace diagram and calculated from the model, respectively.

Table 2. Comparison between Reynolds numbers obtained from Grace diagram (Clift et al.; 1978), Re_{exp}, and those obtained from the model, Re_{model}, in different bubble regimes.

Bubble regime	M	Eo	$\mathrm{Re}_{exp.}$	Re_{model}	Case in Fig. 2
spherical	1.42	0.01	1	1.2	A
wobbling	14.52	1×10^{-9}	2100	2200	B
skirted	142.56	1	15	18	C

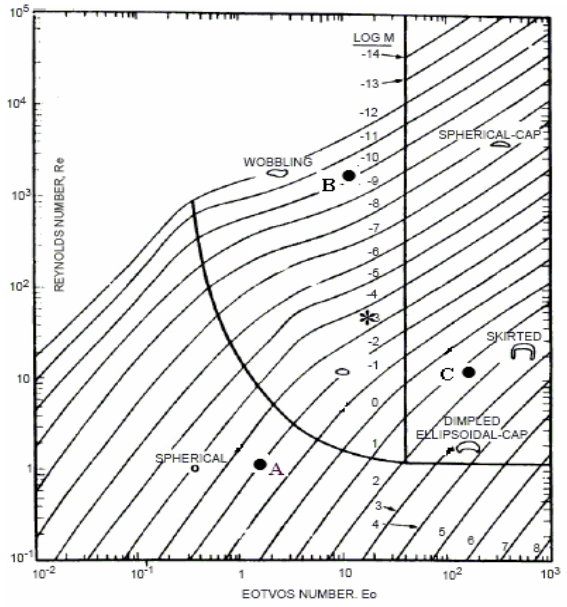

Fig. 2. Grace bubble diagram (Clift et al.; 1978) for the shape and terminal rise velocity of gas bubbles in quiescent viscous liquids.

Effect of Important Parameters

In this section, the effect of different parameters such as tube size, surface tension and viscosity on the shape and rise velocity of the bubble is investigated. In Fig. 3, the effect of tube diameter on the bubble shape and terminal rise velocity is shown. Velocity distributions along with flow streamlines at a time instant are also displayed in the figure. Free-slip boundary conditions were applied at all confining walls. As seen from the figure, increasing the tube diameter increases the rise velocity characterized by Reynolds number. The data used for this simulation are given in Table. 3.

It is well known that surface tension causes an excess pressure inside a bubble given by Laplace equation as $\Delta p = 2\gamma / R$ for a spherical shape, where γ is the surface tension coefficient and R the bubble radius. Figure 4 shows the effect of surface tension on bubble rise velocity. The data used in this simulation are those given in Table 3 except for surface tension which varied from 0.03 N/m to 0.15 N/m. From the figure, it can be clearly seen that the bubble rise velocity increases with liquid surface tension.

Table 3. Data used for the simulation to study the effect of tube diameter.

parameters	liquid	gas
density	ρ_l =1000 kg/m^3	ρ_g =10 kg/m^3
viscosity	μ_l =0.1 kg/(m.s)	μ_a =0.001 kg/(m.s)
surface tension	γ =0.0673 N/m,	-
bubble diameter	-	0.01 m

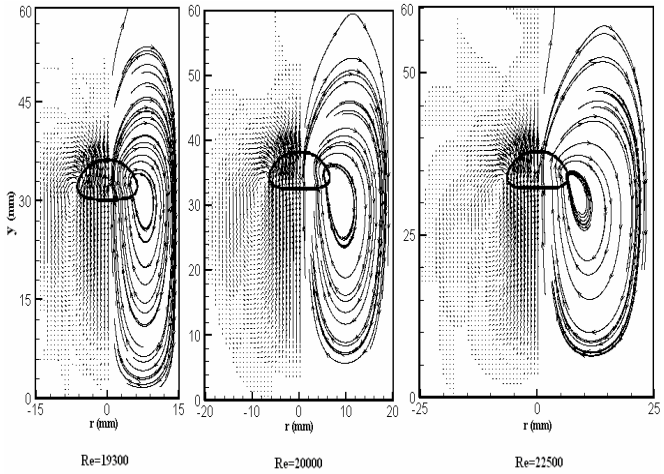

Fig. 3. The effect of tube diameter on bubble shapes and rise velocities.

Figure 5 displays the effect of viscosity on terminal rise velocity for a bubble with an initial diameter of 1 cm. For a given bubble size, the bubble rise velocity is reduced as viscosity ratio is increased. This result was expected because increasing the viscosity ratio decreases the interfacial motion due to viscous forces. The relative reduction in terminal velocity from the maximum to the minimum value also becomes less pronounced as the viscosity ratio increases.

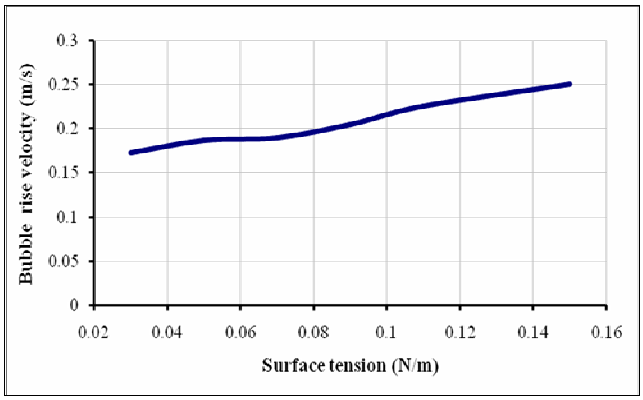

Fig. 4. The variation of bubble rise velocity versus surface tension for a bubble of 0.01 m in diameter.

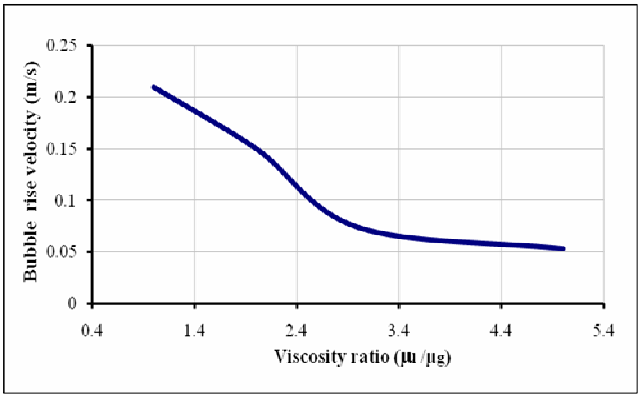

Fig. 5. The variation of bubble rise velocity versus viscosity ratio for a bubble of 0.01 m in diameter.

Interaction and Coalescence of Two Gas Bubbles

Next, we consider the interaction of two gas bubbles that result in their coalescence. In order for two fluid particles to coalesce, the separation distance between them should become much smaller than the size of either particle. The coalescence process can be characterized by three distinct stages as shown in Fig 6. The first stage is the closing approach of the two bubbles or drops to form a thin liquid film between them. The second stage is film thinning or drainage, wherein the liquid film thickness is gradually reduced. Thinning of the film is primarily driven by gravity and capillary forces, and can be significantly affected by the physical properties of the bulk phases and the interfacial tension. Once the film becomes sufficiently thin, it eventually ruptures, thereby leading to coalescence.

Figure 7 shows the sequence of coalescence of two co-axial air bubbles that were initially spherical with a diameter of 1 cm in a quiescent liquid with their centers separated by a distance three times as much as the bubble radius. In the figure, the shape evolution of the two bubbles is shown together with photographs of the experimentally observed bubble shapes (Brereton and Korotney, 1991) just before and after the coalescence process. A very close qualitative agreement is seen between the calculated images and photographs in the same instances of the process.

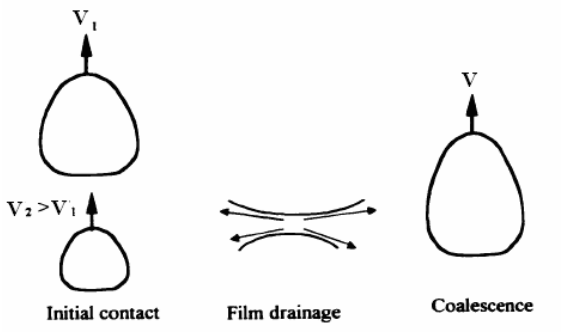

Fig. 6. The three stages of coalescence: initial contact, film drainage, and film rupture.

The sequence of images shows the trailing air bubble approaching the leading one and colliding with it in an axisymmetric configuration to form a doublet. The two air bubbles remain in this configuration with no significant changes in their shapes until the thin film ruptures and the two bubbles coalesce into a single air bubble. When the initial separation distance between centers of the two air bubbles is greater than four times as much of their diameter, the bubbles translate and deform independent of each other. Each air bubble achieves a steady axisymmetric shape which is the same as that observed for a single bubble. Figure 7 shows that the shape of the leading air bubble remains unchanged even as the trailing bubble approaches its trailing end.

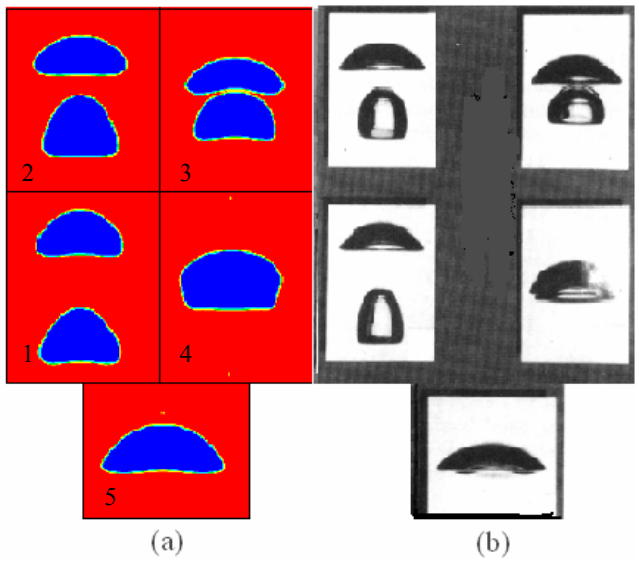

Fig. 7. The co-axial coalescence of two initially spherical bubbles of 0.01 m in diameter during their rise in a quiescent liquid using a) numerical model and b) experiments (Brereton and Korotney, 1991).

Calculated pressure distribution along with flow streamlines at an instance of the process is presented in Fig. 8. The flow recirculation around the bubbles and irregularities of the pressure due to the surface tension effects close to the bubble interfaces are visible in the figure. The hydrostatic pressure variation of the liquid is due to the elevation (y in the figure) and gravity being in the negative y direction. Inside the bubbles, however, the pressure is nearly uniform because the gas density is much less than that of the liquid.

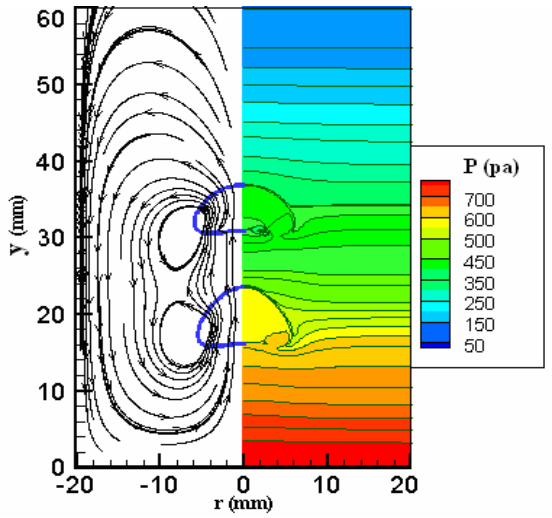

Fig. 8. Calculated pressure distribution and flow streamlines at an instance during the rise and interaction of two bubbles in a viscous liquid.

The coalescence behavior of gas bubbles can be characterized by a value known as the coalescence time. In this study, we define this time as the elapsed time from the instant the two bubbles are in one radius apart up to the instant they coalesce. Figure 9 shows the coalescence time against the dimensionless inter-bubble distance defined as the distance between centers of the two bubbles divided by the bubble radius.

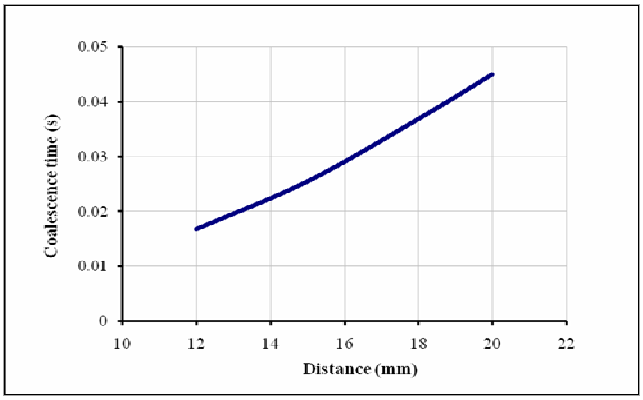

Fig. 9. Coalescence time versus dimensionless inter-bubble distance for bubbles of 1 cm in diameter. The dimensionless inter-bubble distance is defined as the distance between centers of the two bubbles divided by the bubble radius.

From this figure, it can be seen that the coalescence time is a linearly increasing function of the dimensionless inter-bubble distance. Model predictions for the variation of the coalescence time as a function of bubble diameter is shown in Fig. 10 for the buoyancy-driven interaction of two gas bubbles. For simulations corresponding to this figure, centers

of the two bubbles were initially separated by a distance three times as much as the bubble radius. It is seen that as the bubble diameter is increased the two bubbles tend to coalesce in a shorter time.

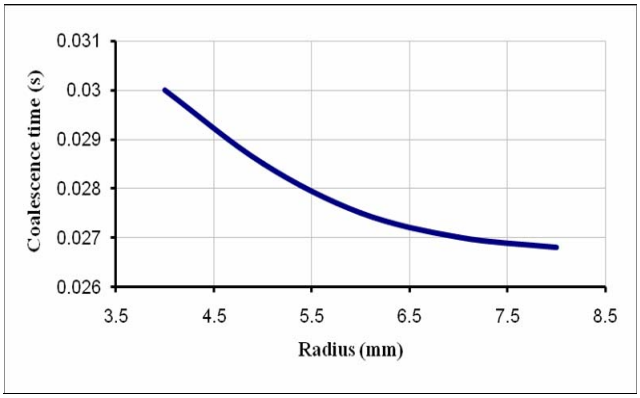

Fig. 10. Coalescence time versus bubble diameter.

CONCLUSION

In this paper, an axisymmetric VOF method was used to simulate the rise and interaction of gas bubbles in a viscous liquid. The model was validated by a comparison between numerical results with available measurements for the bubble deformation and velocity during its rise in a liquid. The effect of increasing diameter on bubble rise velocity was also investigated and compared well with that of the experiment. Next, we investigated the effect of important parameters on the bubble rise velocity. A bubble moving in a narrower tube (smaller diameter) was found to reach a smaller rise velocity. Surface tension and viscosity had adverse effects on the bubble movement. While increasing surface tension raised the bubble rise velocity, increasing liquid viscosity had an opposite effect. Finally, the interaction and coalescence of two axial bubbles during their rise in a quiescent liquid were studied. The calculated images of the coalescence process compared well with those of the experimental photographs. The mechanism behind this phenomenon was found to be the liquid drainage from the space between the two bubbles causing the formation of a thin liquid film and its subsequent rupture resulting in the bubbles coalescence. The two parameters controlling the coalescence are bubbles diameters and the distance between their centers. To characterize this process, we defined a coalescence time as the time elapsed from the instant the two bubbles were in one radius apart up to their coalescence. When the inter-bubble distance was increased, the coalescence time decreased. On the other hand, increasing the bubble diameter reduced the coalescence time.

NOMENCLATURE

de	equivalent bubble diameter, [m]
Eo	Eotvos number (dimensionless)
f	fractional amount of liquid (dimensionless)
g	gravitational acceleration [m/s^2]
M	Morton number **(**dimensionless)
p	pressure [N/m^2]
R	bubble radius [m]
Re	Reynolds number (dimensionless)
t	time [s]
V	velocity [m/s]
V_∞	terminal bubble rise velocity [m/s]
y	computational domain in y-direction [mm]

Greek letters

ρ	density [kg/m^3]
$\Delta\rho$	density difference [kg/m^3]
μ	dynamic viscosity [kg/(m s)]
γ	surface tension [N/m]
τ	viscous stress tensor [N/m^2]
Δp	pressure difference [N/m^2]

Subscripts and superscripts

l	liquid phase
b	bubble
e	equivalent
g	gas
a	air

REFRENCES

Bhaga, D., and Weber, M. E., 1980, In-line interaction of pair of bubbles in a viscous liquid. *Chem. Eng. Sai*, Vol. 35, p. 2467.

Brereton, G., and Korotney, D., 1991, Coaxial and oblique coalescence of two rising bubbles. In: Sahin, I., Tryggvason, G.(Eds), Dynamics of bubbles and vortices near a free surface, AMD-Vol. 119, ASME, New York.

Bussmann M., Mosthghimi J., and Chandra S., 1999, "On a Three-Dimensional Volume Tracking Model of Droplet Impact," *Phys. Fluid*, Vol. 11, p. 1406.

Chang, Y.C., Hou, T.Y., Merriman, B., Osher, S., 1996, A level set formulation of Eulerian interface capturing methods for incompressible fluid flows. *J. Comput. Phys.*, Vol. 124, pp. 449-464.

Clift, R, and Grace, J.R., Weber, M., 1978, Bubbles, Drops and Particles. Academic Press, New York.

Crabtree, J.R, and Bridgewater, J., 1971, Bubble coalescence in viscous liquids. *Chem. Eng. Sci.*, Vol. 26, p. 839.

Duineveld, P. C., 1998, Bouncing and coalescence of bubble pairs rising at high Reynolds number in pure water or aqueous surfactant solutions; *Appl. Sci. Res*. Vol. 58, pp. 409-439.

Esmaeeli, A., and Tryggvason, G., 1998a, Direct numerical simulation of bubble flows. Part I. Low Reynolds number arrays. *J.Fluid Mech*, Vol. 377, pp. 313–345.

Esmaeeli, A., and Tryggvason, G., 1998b, Direct numerical simulation of bubble flows. Part II. Moderate Reynolds number arrays. *J. Fluid Mech.,*Vol. 385, pp. 325–358.

Fedkiw, R., and Osher, S., 2001, Level-set methods: an overview and some recent results. *J. Comput. Phys.*, Vol. 169, p. 463.

Grace, J.R., 1973, Shapes and velocities of bubbles rising in infinite liquids. *Transactions of the Institution of Chemical Engineering*, Vol. 51, pp. 116–120.

Hirt, C.W., Nichols, B.D., 1981, Volume of fluid (VOF) method for the dynamics of free boundaries. *J. Comput. Phys.*, Vol. 39, p. 201.

Manga, M., and Stone H. A., 1993, Bouyoncy-driven interactions between two deformable viscous drops. *J. Fluid Mech.*, Vol. 256, p. 647.

Narayanan, S., Goossens, L. H. J., and Kossen, N.W.F., 1974, Coalescence of two bubbles rising in line at low Reynolds number. *Chem. Eng. Sci.*, Vol. 29, p.2071.

Noh WF, and Woodward PR. 1976, SLIC (Simple Line Interface Calculation) method. In: Van Vooren AI, Zandbergen PJ, eds. *Lecture Notes in Physics*, Vol. 59. Berlin: Springer-Verlag; 330.

Olbricht, W.L., and Kung, D.M., 1987, The interaction and coalescence of liquid drops in flow through a capillary tube. *Int. Colloid Interface Sci.*, Vol. 120, p.229.

Passandideh-Fard, M., and Roohi, E., 2008 (in print), Transient Simulations of Cavitating Flows using a Modified Volume-of-Fluid (VOF) Technique, *Int. J. of Comput. Fluid Dynamics*.

Rudman, M., 1997, Volume-tracking methods for interfacial flow calculations. International Journal of Numerical Methods in Fluids, Vol. 24, pp. 671–691.

Sethian, J.A., 1996, Level Set Methods. Cambridge University Press, Cambridge, UK.

Sussman M, Fatemi E. 1999, An efficient interface-preserving level set redistancing algorithm and its application to interfacial incompressible fluid flow. *SIAM J. Sci. Comput.,* Vol.20, pp. 1165-1191.

Sussman, M., Smereka, P., 1997, Axi-symmetric free boundary problems. *J. Fluid Mech.*, Vol. 341, pp. 269–294.

Sussman M. and Smereka P. Osher S., 1994, A level set approach for computing solutions to incompressible two-phase flow. *J. Comput. Phys.*, Vol.114, pp. 146-159.

Tryggvasson, G., Bunner, B., Esmaeeli, A., 2001, A front tracking method for the computations of multiphase flow. *J. Comput. Phys.*, Vol. 169 (2), pp. 708–759.

Unverdi SO, Tryggvason G. 1992, A front-tracking method for viscous, incompressible multi-fluid flows. *J. Comput. Phys.*, Vol.100, pp. 25-37.

Van Sint Annaland, M., Dijkhuizen, W., Deen, N. G., and Kuipers, J. A. M., 2006, Numerical Simulation of Behavior of Gas Bubbles Using a 3-D Front-Tracking Method. *American Institute of Chemical Engineers (AIChE J)*, Vol. 52, pp. 99–1

Youngs DL., 1982, Time-dependent multi-material flow with large fluid distortion. In: Morton KW, Bianes MJ, eds. Numerical Methods for Fluid Dynamics. *New York, NY: Academic Press*, pp. 273-285.